Electrochemistry Communications 132 (2021) 107138

Contents lists available at ScienceDirect

Electrochemistry Communications

journal homepage: www.elsevier.com/locate/elecom

High-density and low-roughness anodic oxide formed on SiC in highly concentrated LiCl aqueous solution

Yuki Maeda, Atsushi Kitada, Kuniaki Murase, Kazuhiro Fukami *

Department of Materials Science and Engineering, Kyoto University, Kyoto 606-8501, Japan

ARTICLE INFO

Keywords:
Silicon carbide
Anodic oxide
Concentrated aqueous solution
Hydrate melt

ABSTRACT

The wide bandgap and high carrier mobility of silicon carbide (SiC), as well as its physical and chemical stability, make it a promising material for a number of applications. One of the key requirements for these applications involves oxide formation on SiC. The usefulness of the oxide produced by anodizing is, however, limited since the anodic oxide formed on SiC in the usual dilute aqueous solution has a low density and high surface roughness. Here, we consider a new parameter in anodic oxide formation by focusing on the concentration of free water in the electrolyte, using a highly concentrated aqueous solution. In a concentrated solution, oxygen evolution, which results in a reduction in the density of the oxide, is suppressed, and the rate of formation of anodic oxide at defect sites effectively decreases to reduce the surface roughness. Furthermore, an interfacial layer with a higher density than SiO_2 is formed between SiC and SiO_2, buffering the difference in density between them. As a result, we successfully obtained an anodic oxide with a relatively high density and low surface roughness. This study provides a new approach to improving the properties of the anodic oxide formed on SiC.

1. Introduction

The wide bandgap, high carrier mobility, high stability, and chemical inertness of silicon carbide (SiC) make it a promising material for use in next-generation semiconductor devices [1,2], gas sensors and catalyst supports [3], as well as a substrate for the growth of graphene [4,5]. For such applications, surface processing of SiC, especially oxide formation on SiC, is in high demand and has been studied from the viewpoint of its similarity with Si. However, the technology is not yet fully mature.

There are two approaches to obtaining oxide on SiC: thermal oxidation and anodizing. Thermal oxidation of SiC is a practical method for semiconductor devices, but a large number of defects are induced at the interface between the oxide and SiC due to the presence of C atoms [6]. There is still room for improvement in this method, and many theoretical and experimental studies have been performed to reduce the interfacial layer [7,8]. On the other hand, anodizing is an electrochemical method for surface processing, with the advantage of offering a low-cost and low-temperature process using simple equipment. The anodic oxide produced on SiC, however, has a lot of pores and high surface roughness since gas evolution (water splitting and CO/CO_2 evolution through the oxidation of C in SiC) occurs together with oxide formation [9]. This is the reason why the use of the anodic oxide of SiC is limited to the surface polishing of SiC [10]. Moreover, the number of studies on the anodic oxide of SiC is fewer than that on the thermal oxide of SiC, since some groups have already reported that modifying the anodizing parameters, such as pH, solute, and applied potential, is not very effective in improving the properties of the anodic oxide [11,12]. To broaden the application of anodic oxide on SiC, another approach to reducing the number of pores and roughness of the anodic oxide is urgently required.

In previous reports, the concentration of the electrolyte is relatively low, so there is a large amount of free water available to oxidize SiC [11–15]. In contrast, we focus here on the concentration of "free water" as a new parameter in anodic oxide formation on SiC by using a highly concentrated aqueous solution, in which the concentration of free water is extremely limited. Analysis of the anodic oxide formed in the concentrated solution showed an increase in the density and a reduction in the roughness of the anodic oxide. This paper explains the electrochemical behavior and the improvement in the properties of the anodic oxide formed on SiC in a highly concentrated LiCl aqueous solution.

2. Experimental

The SiC substrate (Air Water Inc.) was single crystal boron-doped (p-

* Corresponding author.
E-mail address: fukami.kazuhiro.2u@kyoto-u.ac.jp (K. Fukami).

https://doi.org/10.1016/j.elecom.2021.107138
Received 14 September 2021; Received in revised form 27 September 2021; Accepted 1 October 2021
Available online 6 October 2021

type) 3C-SiC(1 1 1) on a Si(1 1 1) substrate. SiC film with a thickness of 2.5 μm was fabricated by chemical vapor deposition (CVD) as a heteroepitaxial substrate. Before electrochemical measurements, the substrates were cut into 10 × 10 mm samples and cleaned using the procedure we reported previously [16]. We used a three-electrode electrochemical cell with a circular window (5 mm in diameter) to determine the electrode area. The counter electrode (CE) and the reference electrode (RE) were a platinum rod and Ag/AgCl immersed in saturated aqueous KCl solution, respectively.

To prepare a highly concentrated aqueous solution, anhydrous lithium chloride (LiCl; Nacalai Tesque, extra pure reagent) was dissolved in ultrapure water with a molar ratio of LiCl:H_2O = 1:3 (18.5 mol kg^{-1}). For comparison, we also prepared a dilute aqueous solution with a molar ratio of LiCl:H_2O = 1:50 (1.11 mol kg^{-1}). We chose LiCl as the solute because it is highly soluble in water and neither Li^+ nor Cl^- is involved in oxide formation. Although we tried KF and NH_4F, which also have high solubility in water, the F^- ions attacked the SiO_2, and no anodic oxide was formed.

Electrochemical measurements were conducted with a potentiogalvanostat (Bio-Logic, SP-150) in a dark environment to eliminate the effect of ambient light. To investigate the growth of the anodic oxide, impedance measurements and anodizing were conducted alternately with frequencies from 50 kHz to 5 Hz. To analyze the anodic oxide, we used X-ray reflectivity (XRR; RIGAKU, SmartLab-9K), ellipsometry (FE-5000, Otsuka Electronics), X-ray photoelectron microscopy (XPS; JEOL, JPS-9010TRX), field-emission transmission electron microscopy (FE-TEM, JEOL, JEM-2100F), and atomic force microscopy (AFM; BRUKER, NanoWizard III NW3-XS-O).

3. Results and discussion

3.1. Electrochemical behavior of anodizing in a concentrated solution

This section deals only with anodizing in a concentrated solution. For comparison, details of the anodizing behavior and the analysis of the anodic oxide formed in a dilute solution are available in the Supplementary Information.

On anodizing in LiCl aqueous solution, the possible reactions are oxide formation and gas evolution:

$SiC + 3H_2O \rightarrow SiO_2 + CO + 6H^+ + 6e^-$

$SiC + 4H_2O \rightarrow SiO_2 + CO_2 + 8H^+ + 8e^-$

$2H_2O \rightarrow O_2 + 4H^+ + 4e^-$

$2Cl^- \rightarrow Cl_2 + 2e^-$

Since the amount of free water in the concentrated solution is limited, water splitting (O_2 evolution) is suppressed. Furthermore, Cl_2 evolution occurs at a more positive potential than O_2 evolution (see also Section S1 in the Supplementary Information).

Fig. 1a shows cyclic voltammograms (CVs) for SiC in the dilute and concentrated aqueous solutions at a scan rate of 10 mV s^{-1}. In the dilute solution, one peak appears at around 6.5 V, suggesting anodic oxide growth and passivation. The anodic current keeps flowing even in the back scan, suggesting that the passivation is not complete. Actually, after CV the oxide exhibits cracks, as shown in Fig. S2. By contrast, in the concentrated solution there are one peak at 3.5 V and a plateau from 4.0 V to 5.0 V, with no anodic current above 5.5 V. The current density of the peak at 3.5 V decreases steeply as the potential increases, while the plateau at 4.0–5.0 V is broad and gently decreases toward 5.5 V. This implies that two types of oxide films are formed, corresponding to two specific anodic waves in the concentrated solution. Moreover, the current density is almost zero after the second plateau, suggesting that the oxide formed in the concentrated solution passivates SiC more than that produced in the dilute solution. The onset potential in the concentrated solution shifts in a negative direction. There is no reasonable explanation for this behavior from the viewpoint of the *iR* drop of the oxide and in the solution. It suggests that the potential thermodynamically shifts in the concentrated solution. Since the thermodynamics operating in highly concentrated solutions has not been well established, not only in anodizing reactions but also in other fields of electrochemistry, further electrochemical investigations in highly concentrated solutions are necessary to understand the formation of the anodic oxide.

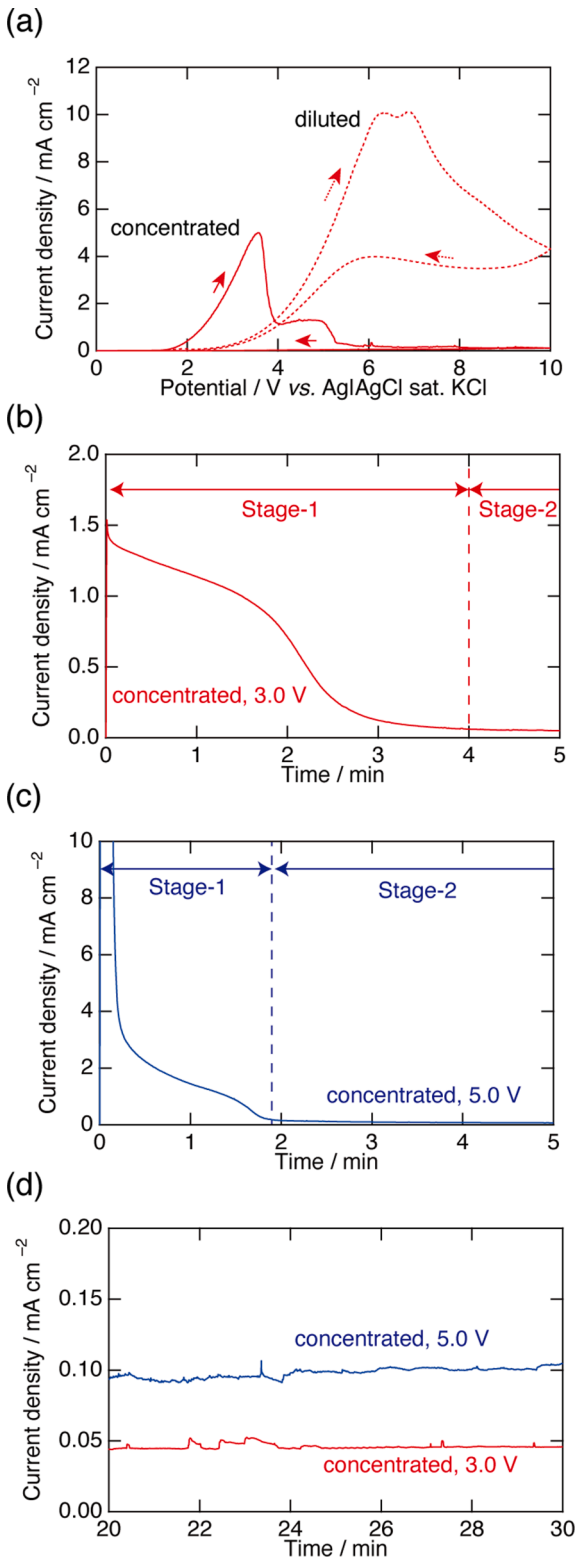

Fig. 1. (a) Cyclic voltammogram for SiC in concentrated (solid line) and dilute LiCl solution (dotted line). Development over time of the current density when SiC was anodized at (b) 3.0 V and (c) 5.0 V in the concentrated solution. (d) Magnification of the time development of the current density in Stage 2.

To discuss the anodic oxide formed in the concentrated solution, we conducted anodizing experiments with constant potentials of 3.0 and 5.0 V, which correspond to the first peak and second plateau in the CV. Fig. 1(b–d) indicates the changes in current density over time during the anodizing. The current density has a plateau at about 1.0–2.0 mA cm^{-2}, and is then reduced and saturated at smaller values. The former plateau region, as well as the latter saturated region, are denoted Stage 1 and Stage 2, respectively. This behavior is observed at both 3.0 and 5.0 V, but the current density is higher, and the duration of Stage 1 is shorter at 5.0 V than at 3.0 V. Also, in Stage 1 at 5.0 V, a large current density (>20 mA cm^{-2}) is observed at the beginning of the anodizing, and the saturated current density at 5.0 V in Stage 2 (Fig. 1d) is larger than that at 3.0 V. This is probably due to Cl_2 evolution in addition to oxide formation and O_2 evolution. Note that gas evolution was observed only at 5.0 V, which suggests that Cl_2 evolution occurs in addition to water splitting at 5.0 V. A detailed discussion of Stages 1 and 2 is given in Section 3.2.

We also conducted electrochemical impedance spectroscopy (EIS) to investigate the growth of the anodic oxide. The resulting Nyquist plots are shown in Fig. 2a and b. The time labels refer to the duration of anodizing. From the obtained Nyquist plots, we calculated the resistance and capacitance of the anodic oxide using an equivalent circuit composed of resistances (R) and a constant phase element (CPE; Q) instead of capacitance (C). Such circuits are commonly used for the analysis of anodic oxide growth [9]. R_1 is the resistance of the electrolyte, and the parallel RQ circuits come from oxide resistance and capacitance. Fig. 2a and b show that the Nyquist plots are composed of one semicircle in Stage 1 but two semicircles in Stage 2. This means that the anodic oxide has one layer in Stage 1 but two layers in Stage 2. Note that the Nyquist plot has two semicircles in both Stage 1 and Stage 2 under an applied potential of 5.0 V, but the Nyquist plot in Stage 1 (Fig. 2(b-2)) is close to one semicircle. Thus, Fig. 2 (b-2) shows the Nyquist plot in the transition region from Stage 1 to Stage 2. The parameters calculated from the Nyquist plots are shown in Fig. 2c and d. R_2 and Q_2, which are due to the oxide formed in Stage 1, are almost constant (Fig. 2c); on the other hand, R_3 and Q_3, which come from the oxide formed in Stage 2, change greatly with increasing anodizing time. The oxide growth causes the resistance to increase and the capacitance (CPE in this experiment) to decrease, as expressed in the equation $C = \varepsilon_r \varepsilon_0 S/d$. Here ε_r and ε_0 are the relative permittivity of the oxide and the permittivity of a vacuum. S and d represent the surface area and thickness of the oxide, respectively. Consequently, one oxide layer with a constant thickness is formed in Stage 1 and another oxide layer keeps growing in Stage 2. Considering the difference between the applied potentials, although the value of R_3 keeps changing at 5.0 V, the value at 3.0 V is saturated after an anodizing period of 15 min. This means that the thickness of the oxide formed at 3.0 V is saturated even in Stage 2. The value of Q_3 also varies between 3.0 and 5.0 V. This suggests that the oxide formed at 3.0 V passivates SiC more than that produced at 5.0 V.

3.2. Analysis of the anodic oxide formed in the concentrated solution

We investigated the thickness, bulk density, crystallinity, chemical state, and surface roughness of the anodic oxide using XRR, ellipsometry, STEM, XPS, and AFM.

First, XRR was performed to investigate the oxide thickness and bulk density. The XRR and its fitting results are shown in Fig. S3. The fitting was conducted with the GlobalFit software (Rigaku Cooperation) until the smallest chi-square (χ^2) value was under 0.01. For the fitting, we assumed the following 3-layer structure: SiO_2, an interfacial layer, and single crystal SiC (3C). The interfacial layer is suggested in the electrochemical impedance spectroscopy as discussed above, and its existence was also reported in XRR and secondary ion mass spectrometry (SIMS) of the thermally produced oxide on 4H-SiC [17]. Note that $\chi^2 \leq 0.01$ could not be achieved when we assumed a two-layer structure involving only SiO_2 and SiC layers. The oxide thickness was also determined by ellipsometry. In ellipsometry, (Ψ, Δ) spectra were fitted using a two-layer structure (SiO_2 and SiC) because the optical constants of ideal SiO_2 and SiC are well-known, but that of the anodic oxide, especially the interfacial layer, is not. For this reason, the residuals of the fitting were high in the ellipsometry results, and the thickness is slightly different from the values calculated from XRR. The calculated thickness and density are summarized in Table 1, indicating that SiO_2 and the interfacial layer are formed in Stage 1, and only a SiO_2 layer is grown in Stage 2. In addition, the density of the interfacial layer is higher than that of amorphous SiO_2 (ρ = 2.2 g cm^{-3}). This result coincides with that of

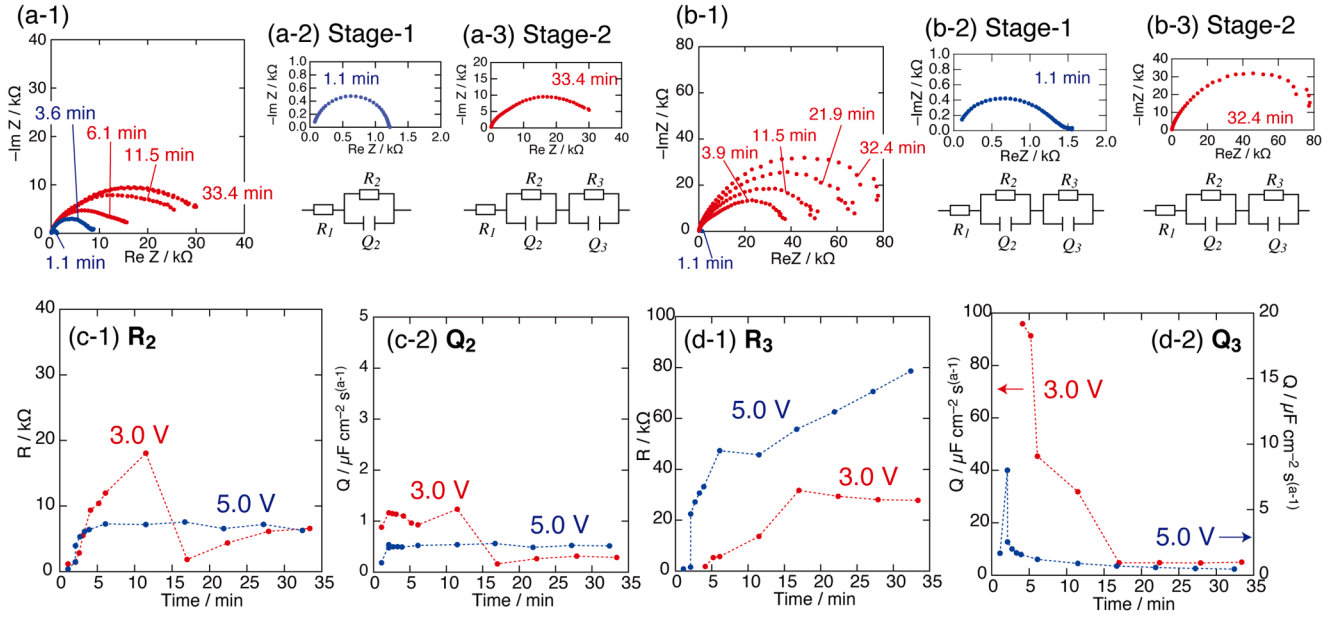

Fig. 2. Nyquist plots measured at (a) 3.0 V and (b) 5.0 V in the concentrated solution. The time labels indicate the duration of the anodizing. The blue and red markers show the Nyquist plots corresponding to Stage 1 and Stage 2, respectively. The equivalent circuits used are shown below each Nyquist plot. The time dependence of (c-1 and d-1) R (resistance) and (c-2 and d-2) Q (constant phase element) were calculated from the Nyquist plots shown in Fig. 2a and b. (For interpretation of the references to colour in this figure legend, the reader is referred to the web version of this article.)

Table 1
Ellipsometry and XRR results for the anodic oxide on SiC in the concentrated solution. The SiO_2 thickness was calculated with ellipsometry, assuming the samples are composed of two layers (SiO_2 and SiC). The thickness and the density of each layer were also calculated from XRR, assuming three layers (SiO_2, interface, SiC).

Applied potential/V	Stage	Charge density/C cm^{-2}	Ellipsometry	XRR				
			Thickness/nm	Thickness/nm			Density/g cm^{-3}	
			SiO_2	Total	SiO_2	Interface	SiO_2	Interface
3.0	Stage 1	0.31	7.32	5.44	3.67	1.77	0.89	1.95
	Stage 2	0.50	52.75	52.19	50.78	1.41	1.26	2.82
5.0	Stage 1	0.50	14.12	7.97	4.97	3.00	0.69	2.73
	Stage 2	0.59	56.93	46.19	43.63	2.56	0.37	2.67

thermal oxide formation, where an interfacial layer with a high density is assumed to be SiO_xC_y [17]. Though the density of the SiO_2 layer formed at 3.0 V ($\rho = 1.26$ g cm^{-3}) is higher than that at 5.0 V, both are lower than that of amorphous SiO_2. In the dilute solution, however, the density of SiO_2 is quite low ($\rho = 0.58$ g cm^{-3}) and the interfacial layer is negligible in the dilute solution, as discussed in Section S4 of the Supplementary Information. Thus, we conclude that the concentrated solution makes it possible to fabricate a high-density anodic oxide by selecting a suitable applied potential. The charge density during anodizing is also shown in Table 1. The charge in Stage 1 at 5.0 V is the same as that in Stage 2 at 3.0 V since the large current density is observed at 5.0 V in Stage 1 (Fig. 1c). The oxide thickness in Stage 1 at 5.0 V, however, is quite a lot smaller than that in Stage 2 at 3.0 V. This means that the high current density of Stage 1 at 5.0 V mainly comes from Cl_2 evolution due to the extremely high concentration of Cl^- ions. Note that it is difficult to obtain an accurate value of the efficiency of anodizing since the theoretical numbers of charge carriers in the oxidation reactions from SiC to the interfacial layer and from the interfacial layer to SiO_2 have not yet been clarified. Nevertheless, a set of rough efficiency values is summarized in Table S2. It shows that the current efficiency in both Stages 1 and 2 at 5.0 V is low, suggesting that the Cl_2 evolution occurs in addition to the O_2 evolution, but the current efficiency in Stage 2 at 3.0 V is relatively high. This indicates that the gas evolution reactions, which cause the reduction in the density of the oxide, are effectively suppressed at 3.0 V in the concentrated solution.

Next, we discuss the crystallinity and chemical state of the anodic oxide in Stage 2 from the XPS spectra and cross-sectional STEM images shown in Fig. 3. The XPS spectra were calibrated according to C 1s band, using the signal for C–C (285.0 eV) peak. Fig. 3a shows that the anodic oxide is confirmed to be SiO_2. Other peaks were detected in the C 1s and Cl 2p spectra. The peaks in the C1s spectrum are assigned to C–C, C–OH, and COOH, which are attributed to anodized carbon in SiC and carbon contamination. This suggests that SiO_xC_y, which exists in the SiO_2/SiC interface, gradually transitions to SiO_2 as C is removed as CO and/or CO_2. In the Cl 2p spectrum, the small peaks, which are assigned not to LiCl (199 eV) but C–Cl (200.5 and 202.1 eV: Cl $2p_{3/2}$ and $2p_{1/2}$, respectively [18]), are observed. The peak exists only on the outermost surface, as shown in Fig. S4, and thus this comes from an intermediate in Cl_2 evolution. The cross-sectional STEM bright-field images and nanobeam electron diffraction results indicate that samples obtained at both 3.0 V and 5.0 V have an amorphous SiO_2 layer. The interfacial layer, which was proposed by EIS and XRR, was not detected, suggesting that it was thin and gradually changed to SiO_2. In Fig. 3c, the SiO_2 layer formed at 5.0 V has dark spots, which EDS analysis showed to contain gallium (Ga). This Ga comes from sample preparation with a focused ion beam (FIB), which uses Ga ions for sputtering. Presumably some of the Ga ions were trapped in the small pores in SiO_2 formed at 5.0 V. Since gas evolution (mainly Cl_2 evolution) seems to occur not at 3.0 V but at 5.0 V, the gas evolution and diffusion develop the pores to cause further degradation of the density of the anodic oxide at 5.0 V. In the case of the dilute solution, the density of the anodic oxide is even lower since O_2 evolution occurs in addition to Cl_2 evolution. Note that pores are not recognized with TEM in the sample anodized at 3.0 V, although its density is lower than that of amorphous SiO_2. This suggests that the size and number of pores formed at 3.0 V are too small to be observed using TEM. Consequently, the suppression of gas evolution by controlling the concentration of free water and the applied potential is significant in the formation of a high-density anodic oxide.

Finally, we focus on the surface roughness of the anodic oxide in Stage 2 using AFM. The root mean square (RMS) roughness of the oxides formed at 3.0 and 5.0 V are 19.55 nm and 20.17 nm, respectively. Since the RMS of the original SiC is 17.66 nm, the surface roughness of the anodic oxide is almost the same as that of the original SiC. Fig. 4 shows AFM images of the original SiC, and the anodic oxides formed at 3.0 V and 5.0 V. All surfaces feature triangular shapes of various sizes, which means that anodic oxide formation occurs homogeneously in the concentrated solution. This shape is formed during single-crystal SiC deposition by CVD and results from the emerging (1 1 1) plane, which is the most stable plane of 3C-SiC. By contrast, in the dilute solution the surface is covered with protruding SiO_2, as shown in Fig. S8, and the RMS roughness is 25.13 nm. The difference in the RMS roughness is small, but the surface morphology is totally changed in the dilute solution. To increase the difference in the surface roughness, anodizing (oxide formation) and HF etching (oxide removal) were conducted repeatedly. A detailed discussion of this is given in Section S5. The results indicate that the roughness of the anodic oxide formed in the concentrated solution is almost constant, even after repeated anodizing. On the other hand, the roughness of the anodic oxide produced in the dilute solution is greatly increased (Fig. S12). This means that the concentrated solution reduces the surface roughness of the anodic oxide by preventing the formation of the protruding SiO_2. Anodic oxide formation on SiC in dilute solutions has been investigated in various different solutions. Examples include 20 wt% HCl, NaCl, $NaNO_3$, and NaOH [11], 1 wt% NaCl [13,14], 0.13 M KCl [12], molten KOH [19], and 0.1 M H_3PO_4 [15]. In these reports, the roughness of the oxide increases with anodizing due to the formation of protruding SiO_2, since oxidation preferentially occurs on surface defects and atomic pits [14], and the difference between the density of SiO_2 (<2.2 g cm^{-3}) and SiC (3.21 g cm^{-3}) is high. In contrast, the oxidation rate is slow in both defect-rich areas and areas without defects in the concentrated solution, due to the lack of free water. Also, SiO_xC_y, which has a density relatively close to that of SiC, is formed between SiC and SiO_2 as a buffer. As a result, SiO_2 with a low surface roughness is obtained in the concentrated solution.

3.3. Model of anodic oxide formation in the concentrated solution

To summarize the previous sections, anodizing in a concentrated solution produces an anodic oxide with a higher density and lower roughness than anodizing in a dilute solution. Moreover, the anodic oxide has two layers, SiO_xC_y and SiO_2. The SiO_xC_y layer has a strong passivation effect on SiC. Fig. S13 shows a scheme representing the anodizing of SiC in a concentrated solution. In Stage 1, SiC is partially oxidized to SiO_xC_y by the diffusion of H_2O toward the SiC surface, and H^+ ions are released to the layer (Stage 1). After passivation by the SiO_xC_y layer, SiO_xC_y is gradually oxidized to SiO_2 by the diffusion of carbon atoms from SiO_xC_y and H_2O from the electrolyte. Since the formation rate of SiO_xC_y is balanced with that of SiO_2, only the thickness of

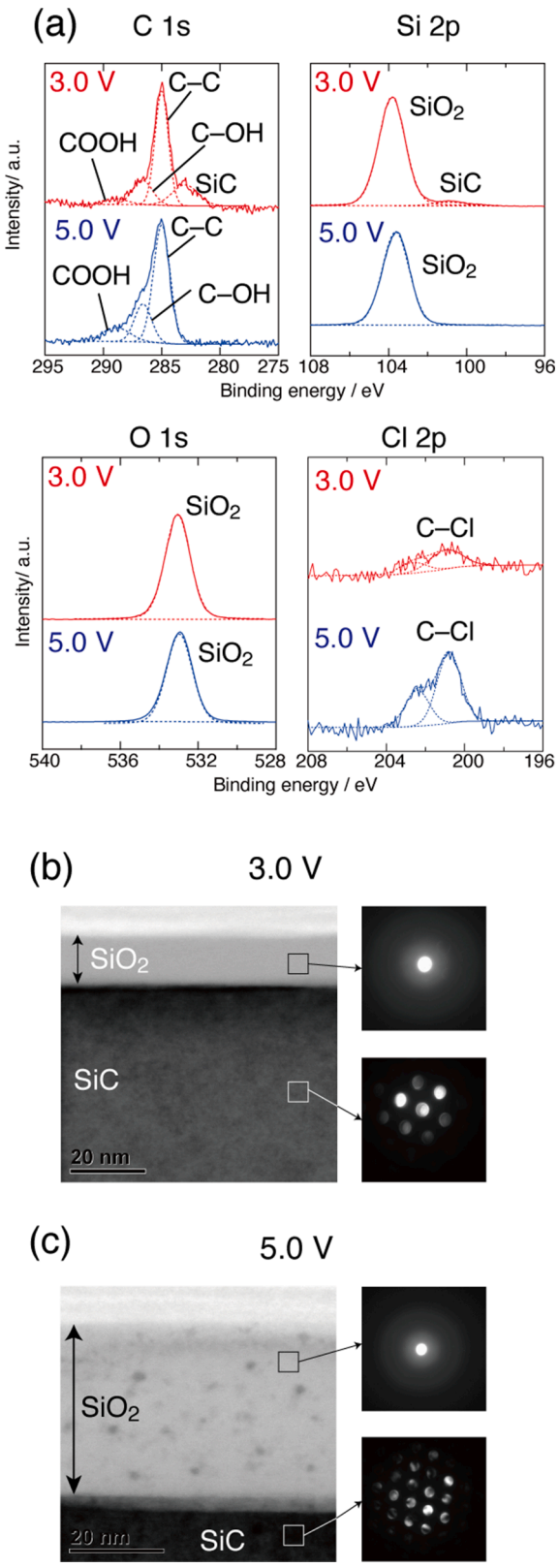

Fig. 3. (a) XPS spectra of SiC anodized at 3.0 V (red) and 5.0 V (blue) in the concentrated solution. STEM bright-field images and nano-beam electron diffraction of the samples anodized at (b) 3.0 V and (c) 5.0 V in the concentrated solution. (For interpretation of the references to colour in this figure legend, the reader is referred to the web version of this article.)

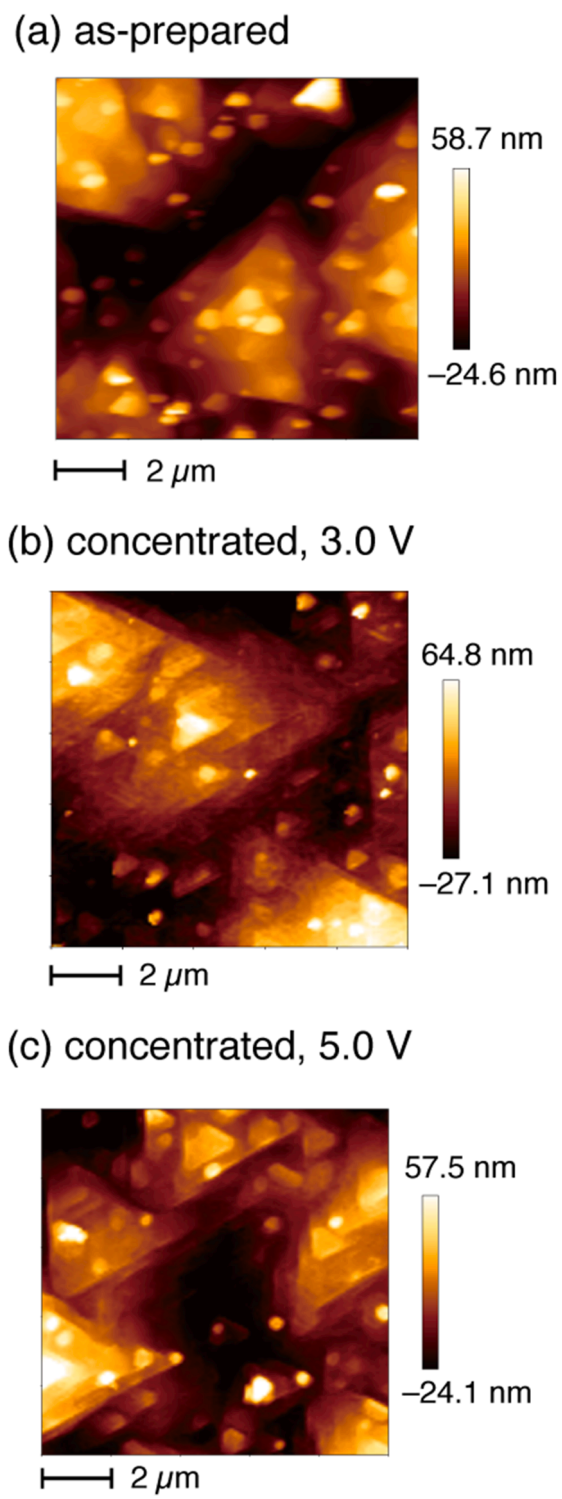

Fig. 4. AFM images of (a) original SiC and (b, c) anodized SiC. The anodizing was conducted at (b) 3.0 V and (c) 5.0 V in the concentrated solution.

SiO_2 increases (Stage 2). When SiO_xC_y is oxidized to SiO_2 by H_2O, CO/CO_2 is released from the interface to the electrolyte as a gas phase. The gas evolution and diffusion produces pores in the SiO_2 layer, thus explaining the fact that the density of SiO_2 is lower than the theoretical value of amorphous SiO_2. Additionally, since Cl_2 gas evolution also occurs at 5.0 V, the density of the oxide formed at 5.0 V is lower than that produced at 3.0 V. In a dilute solution, the transition from SiO_xC_y to SiO_2 is rapid due to the abundance of free water, and much more gas

evolution occurs at the same time. As a result, the SiO_xC_y layer is not detected and the density of SiO_2 is quite low. Considering the CV in Fig. 1a, the first peak is assigned to SiO_xC_y formation and passivation. After SiO_2 formation and Cl_2 evolution after the first peak, a SiO_2 layer containing pores is formed at the second plateau. Since the thickness of SiO_2 increases as the potential is scanned, passivation occurs again with SiO_2.

4. Conclusions

We investigated anodic oxide formation in a concentrated aqueous solution. Anodizing in concentrated LiCl solution produces an anodic oxide with a higher density and a lower surface roughness on SiC than in a dilute solution. The increase in the density is a result of the suppression of O_2 evolution by the depletion of free water. The applied potential is significant in producing a high-density anodic oxide since Cl_2 evolution causes pore formation. Additionally, the concentrated solution reduces the surface roughness of the anodic oxide. This is because the oxidation rate at defect sites is effectively slow, and the interfacial layer, which has a higher density than SiO_2, acts as a buffer between SiC and SiO_2. In this paper, we demonstrated the effect of the concentration of free water on anodic oxide formation on SiC. We believe that this study suggests a pathway for further research into anodizing in concentrated aqueous solutions, which has great potential for electrochemical surface processing.

CRediT authorship contribution statement

Yuki Maeda: Investigation, Validation, Writing - original draft, Funding acquisition. **Atsushi Kitada:** Validation, Writing - review & editing. **Kuniaki Murase:** Validation, Writing - review & editing, Funding acquisition. **Kazuhiro Fukami:** Conceptualization, Methodology, Writing - original draft, Supervision, Project administration, Funding acquisition.

Declaration of Competing Interest

The authors declare that they have no known competing financial interests or personal relationships that could have appeared to influence the work reported in this paper.

Acknowledgments

This work was supported by a JSPS Grant-in-Aid for Scientific Research B (Grant Number 21H01670; K.F.), JSPS KAKENHI Fostering Joint International Research B (Grant Number 20KK0122; K.F.), a Grant-in-Aid for Scientific Research S (Grant Number 20H05663; K.M.), and a Grant-in-Aid for JSPS Fellows (Grant Number 21J14738; Y.M.).

Appendix A. Supplementary data

Supplementary data to this article can be found online at https://doi.org/10.1016/j.elecom.2021.107138.

References

[1] H. Matsunami, T. Kimoto, Mater. Sci. Eng. R: Reports 20 (1997) 125–166.
[2] D. Nakamura, I. Gunjishima, S. Yamaguchi, T. Ito, A. Okamoto, H. Kondo, S. Onda, K. Takatori, Nature 430 (2004) 1009–1012.
[3] K.S. Kim, G.S. Chung, Sensors Actuators B Chem. 157 (2011) 482–487.
[4] K.V. Emtsev, A. Bostwick, K. Horn, J. Jobst, G.L. Kellogg, L. Ley, J.L. McChesney, T. Ohta, S.A. Reshanov, J. Röhrl, E. Rotenberg, A.K. Schmid, D. Waldmann, H. B. Weber, T. Seyller, Nat. Mater. 8 (2009) 203–207.
[5] J. Robinson, X. Weng, K. Trumbull, R. Cavalero, M. Wetherington, E. Frantz, M. LaBella, Z. Hughes, M. Fanton, D. Snyder, ACS Nano 4 (2010) 153–158.
[6] V.V. Afanasev, M. Bassler, G. Pensl, M. Schulz, Phys. Status Solidi 162 (1997) 321–337.
[7] T. Kobayashi, T. Okuda, K. Tachiki, K. Ito, Y. Matsushita, T. Kimoto, Appl. Phys Express 13 (2020), 091003.
[8] T. Kobayashi, K. Harada, Y. Kumagai, F. Oba, Y. Matsushita, J. Appl. Phys. 125 (2019), 125701.
[9] D.H. van Dorp, E.S. Kooij, W. Arnoldbik, J.J. Kelly, Chem. Mater. 21 (2009) 3297–3305.
[10] H. Deng, K. Hosoya, Y. Imanishi, K. Endo, K. Yamamura, Electrochem. Commun. 52 (2015) 5–8.
[11] Z. Chen, Y. Zhao, Electrochem. Commun. 109 (2019), 106608.
[12] N. Liu, R. Yi, H. Deng, Electrochem. Commun. 89 (2018) 27–31.
[13] X. Yang, R. Sun, K. Kawai, K. Arima, K. Yamamura, ACS Appl. Mater. Interfaces 11 (2019) 2535–2542.
[14] X. Yang, R. Sun, Y. Ohkubo, K. Kawai, K. Arima, K. Endo, K. Yamamura, Electrochim. Acta 271 (2018) 666–676.
[15] W.S. Woon, S.D. Hutagalung, K.Y. Cheong, Thin Solid Films 517 (2009) 2808–2812.
[16] Y. Maeda, K. Fukami, S. Kondo, A. Kitada, K. Murase, T. Hinoki, Electrochem. Commun. 91 (2018) 15–18.
[17] P. Kamiński, R. Budzich, J. Gaca, P.P. Michałowski, R. Kozłowski, A. Harmasz, T. Ciuk, J. Płocharski, J. Mater. Chem. C 9 (2021) 4393–4404.
[18] J.M. González-Domínguez, P. Castell, S. Bespín-Gascón, A. Ansón-Casaos, A. M. Díez-Pascual, M.A. Gómez-Fatou, A.M. Benito, W.K. Maser, M.T. Martínez, J. Mater. Chem. 22 (2012) 21285.
[19] Y. Zhang, H. Chen, D. Liu, H. Deng, Appl. Surf. Sci. 525 (2020), 146532.